(2)

ABSOLUTE TWO-PHOTON ABSORPTION COEFFICIENTS IN ULTRAVIOLET WINDOW MATERIALS

N. Bloembergen, Principal Investigator, 617/495-3936
J. Blake, Program Manager, 617/495-4585

Harvard University
Cambridge, Massachusetts 02138

FINAL TECHNICAL REPORT

Covering the Period
June 1, 1975 - September 30, 1977

Contract No. F44620-75-C-0086

Effective Date: June 1, 1975
Expiration Date: September 30, 1977

Sponsored by

Advanced Research Projects Agency (DOD)
ARPA Order No. 2983
Monitored by NE Under Contract No. F44620-75-C-0086

Unclassified

SECURITY CLASSIFICATION OF THIS PAGE (When Data Entered)

(19) REPORT DOCUMENTATION PAGE

READ INSTRUCTIONS BEFORE COMPLETING FORM

(18) 1. REPORT NUMBER: AFOSR-TR-78-0051

2. GOVT ACCESSION NO.

3. RECIPIENT'S CATALOG NUMBER (9)

(6) 4. TITLE (and Subtitle): ABSOLUTE TWO-PHOTON ABSORPTION COEFFICIENTS IN ULTRA VIOLET WINDOW MATERIALS.

5. TYPE OF REPORT & PERIOD COVERED: Final Technical Report. 1 Jun 75 - 30 Sep 77

6. PERFORMING ORG. REPORT NUMBER

(10) 7. AUTHOR(s): N./Bloembergen, J./Blake

8. CONTRACT OR GRANT NUMBER(s): (15) F44620-75-C-0088, ARPA Order-2983

9. PERFORMING ORGANIZATION NAME AND ADDRESS: Division of Applied Sciences, Harvard University, Cambridge, Mass. 02138

10. PROGRAM ELEMENT, PROJECT, TASK AREA & WORK UNIT NUMBERS: 61102F, A02983

11. CONTROLLING OFFICE NAME AND ADDRESS: Advanced Research Projects Agency (DOD), 1400 Wilson Boulevard, Arlington, Virginia 22209

12. REPORT DATE: (11) Dec 77

13. NUMBER OF PAGES: (12) 58P.

14. MONITORING AGENCY NAME & ADDRESS (if different from Controlling Office): Air Force Office of Scientific Research/NE, Bolling Air Force Base, Washington, D.C. 20332

15. SECURITY CLASS. (of this report): Unclassified

15a. DECLASSIFICATION/DOWNGRADING SCHEDULE

16. DISTRIBUTION STATEMENT (of this Report)

Approved for public release; distribution unlimited.

17. DISTRIBUTION STATEMENT (of the abstract entered in Block 20, if different from Report)

18. SUPPLEMENTARY NOTES

19. KEY WORDS (Continue on reverse side if necessary and identify by block number)

Alkali Halides
Breakdown Damage
Calcium Fluoride
Harmonic Generating Crystals .0001
Nonlinear Absorption
Quartz
Sapphire
Ultraviolet Window Materials
Ultraviolet Two-Photon Absorption .001

20. ABSTRACT (Continue on reverse side if necessary and identify by block number)

The absolute two-photon absorption coefficients of u.v. transmitting materials have been measured using well-calibrated single picosecond pulses, at the third and fourth harmonic of a mode locked Nd:YAG laser systems. Two-photon absorption coefficients of the order of 10^{-3} cm/MW were measured for alkali-halides, and 10^{-4} cm/MW for harmonic generating crystals. In materials with band gap greater than $2\hbar\omega$, no nonlinear absorption could be observed. Calculations based on the Keldysh theory with one adjustable parameter agree quite well with the experimentally observed dispersions in the

→ next page

DD FORM 1 JAN 73 1473 EDITION OF 1 NOV 65 IS OBSOLETE S/N 0102-014-6601

h-bar omega

410 457

Unclassified

20. Abstract continued

two-photon absorption coefficients. The effect of multi-photon absorption on the conversion efficiency of harmonic generating crystals and on the breakdown of u. v. window materials is also discussed.

PREFACE

This final technical report summarizes the work, performed under Contract Number F44620-75-C-0088 at Harvard University during the period June 1, 1975 - September 30, 1977.

Work in the area of laser induced breakdown and multiphoton absorption in ultraviolet and infrared laser window materials was carried out during the entire period, with N. Bloembergen as principal investigator. A brief summary is given in Section A, with ample references to previously issued reports and publications. A detailed account of the results obtained during the final semiannual reporting period, April 1 - September 30, 1977 is contained in Section B.

Support for work in the area of superconducting materials was discontinued in September 1976. A final report on this work was distributed at that time. In Section C the principal investigator, Professor M. Tinkham, provides a summary.

Support for work in the area of fracture mechanics was discontinued in September 1976. A final report on this work was distributed at that time. In Section C the principal investigator, Professor J. R. Hutchinson, provides a brief summary of this area.

The investigators contributing to this final report are:

Professor N. Bloembergen, Principal Investigator
Professor J. R. Hutchinson, Principal Investigator
Professor M. Tinkham, Principal Investigator
Dr. J. H. Bechtel, Former Research Fellow
Dr. H. Lotem, Research Fellow
Dr. W. Lee Smith, Former Research Fellow and Graduate Student
Mr. P. Liu, Graduate Student.

The views and conclusions contained in this document are those of the authors and should not be interpreted as necessarily representing the official policies, either expressed or implied, of the Defense Advanced Research Projects Agency or the U.S. Government.

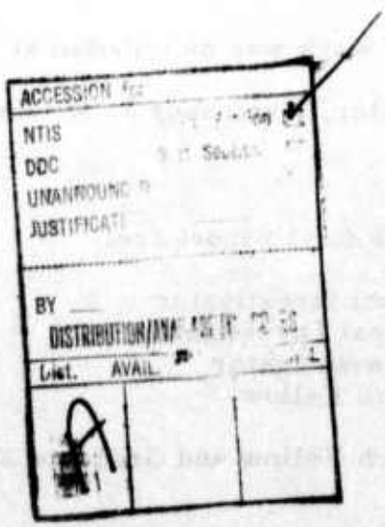

A. SUMMARY OF WORK ON LASER INDUCED BREAKDOWN AND MULTIPHOTON ABSORPTION IN UV WINDOW MATERIALS.

Professor N. Bloembergen, Principal Investigator.

The intrinsic mechanisms of avalanche ionization and multiphoton absorption in optical materials transparent in the ultraviolet have been investigated. This work is relevant to the development of high power excimer lasers operating at ultraviolet wavelength, to elucidate the causes of failure of UV windows and coatings.

It has been shown that the damage threshold of the intrinsic window material, excluding absorbing impurities, increases by a factor two or three in going from the infrared to the visible, then reaches a maximum and decreases in the ultraviolet region. This qualitative trend can be explained by the creation of an absorbing carrier plasma. The threshold at lower frequencies is mostly determined by avalanche ionization, at higher frequencies by multiphoton absorption.

The breakdown threshold data have been discussed extensively in previous technical reports[1,2] and in several publications.[3-5]

This material will not be reviewed again, as Technical Report[1] No. 665 "Dielectric Breakdown Induced by Picosecond Laser Pulses" received a wide distribution.

The techniques of the measurement of two-photon absorption cross sections and preliminary results have also been discussed in the previous semiannual technical reports, as well as in several publications.[6-10] Extensive results on two-photon absorption cross sections in a large number of UV window materials, as well as in

several harmonic generating crystals, including KDP, ADP and others, have been obtained more recently. These are presented in detail in Section B of this report. This same material has also been submitted for publication in the Physical Review.

The results show that the two-photon absorption cross sections are smaller than 10^{-5} cm/W, if the band gap of the material is larger than twice the photon energy. It may be concluded that intrinsic multi-photon absorption is not responsible for the damage occurring at present in high power UV laser systems. The damage in coatings and windows in these systems must be caused by one-photon absorption due to impurities and color centers.

The intrinsic two-photon absorption cross section in transparent materials with a bandgap between $\hbar\omega$ and $2\hbar\omega$, lies in the range of 3×10^{-3} to 3×10^{-5} cm/MW. It is fortunate that sapphire, quartz and the harmonic generating crystals have cross-sections at the lower end of this range, so that they are still quite useful in the frequency range $2\hbar\omega > E_{gap} > \hbar\omega$. Further details are given in the next section.

The following publications and reports were supported in part by this contract.

1. W. L. Smith, J. H. Bechtel and N. Bloembergen, Dielectric Breakdown Induced by Picosecond Laser Pulses, Technical Report No. 665, Harvard University, October, 1976.

2. W. L. Smith, J. H. Bechtel and N. Bloembergen, "Picosecond Breakdown Studies: Threshold and Nonlinear Index Measurements and Damage Morphology," in National Bureau of Standards, Special Publication No. 435, edited by A. J. Glass and A. Guenther, p. 321, 1975.

3. W. L. Smith, J. H. Bechtel and N. Bloembergen, "Picosecond laser induced damage morphology," Optics Comm. 18, 592, 1976.

4. W. L. Smith, J. H. Bechtel and N. Bloembergen, "Picosecond laser-induced breakdown at 5321 and 3547 A: Observation of frequency dependent behavior," Phys. Rev. B15, 4039, 1977.

5. W. L. Smith, P. Liu and N. Bloembergen, "Superbroadening in H_2O and D_2O by self-focused picosecond pulses from a YAlG:Nd laser," Phys. Rev. A15, 2396, 1977.

6. J. H. Bechtel and W. L. Smith, "Pulse width fluctuations in mode-locked lasers," Phys. Lett. 55A, 203, 1975.

7. J. H. Bechtel and W. L. Smith, "Two-photon absorption in semiconductors with picosecond laser pulses," Phys. Rev. 13, 3515, 1976.

8. W. L. Smith and J. H. Bechtel, "A simple technique for individual picosecond laser pulse duration measurements," J. App. Phys. 47, 1065, 1976.

9. J. H. Bechtel and W. L. Smith, "Two-photon fluorescence in attenuating media," J. App. Phys. 46, 5055, 1976.

10. H. Lotem and Cid B. de Araujo, "Absolute determination of the two-photon absorption coefficient relative to the inverse Raman cross section," Phys. Rev. B16, 1711, 1977.

11. E. Yablonovitch and H. S. Kwok, "Electrical triggering of an optical breakdown plasma with subnanosecond jitter, Appl. Phys. Lett. 27, 583, 1975.

B. ABSOLUTE TWO-PHOTON ABSORPTION COEFFICIENTS AT 355 AND 266 nm.

Professor N. Bloembergen, Principal Investigator.

The absolute two-photon absorption coefficients of u.v. transmitting materials have been measured using well-calibrated single picosecond pulses, at the third and fourth harmonic of a mode locked Nd:YAG laser system. Two-photon absorption coefficients of the order of 10^{-3} cm/MW were measured for alkali-halides, and 10^{-4} cm/MW for harmonic generating crystals. In materials with band gap greater than $2\hbar\omega$, no nonlinear absorption could be observed. Calculations based on the Keldysh theory with one adjustable parameter agree quite well with the experimentally observed dispersions in the two-photon absorption coefficients. The effect of multi-photon absorption on the conversion efficiency of harmonic generating crystals and on the breakdown of u.v. window materials is also discussed.

I. Introduction

The first theoretical study on two-photon absorption (TPA) process was carried out by Maria Goppert-Mayer[1] in 1931. With the advent of the ruby lasers Kaiser and Garrett[2] observed TPA at optical frequencies in 1961. Several techniques have subsequently been used to find TPA coefficients, for example, by measuring the intensity dependent transmission through two-photon excitation. Several comprehensive reviews of TPA are available.[3-5]

Absolute TPA coefficients can only be obtained directly by well-calibrated lasers. However, relative measurements can be done quite simply by the two-channel technique.[6] The same technique may also be used to obtain absolute TPA coefficients by utilizing known Raman cross sections.[7] Since the TPA coefficient is related to the imaginary part of the third order nonlinear susceptibility, parametric mixing experiments such as three-wave mixing which are capable of measuring the real and imaginary part of the third-order nonlinear susceptibility have been used to find TPA cross section.[8]

TPA studies have both scientific and technological interest. Because the TPA selection rules are different in general from the linear spectroscopy selection rules, TPA data may provide new information about electronic wave functions and energy levels in the material. In particular, additional information on band structure in solids may be obtained. Practically, the TPA process has been used to excite bulk carriers in large semiconductor crystals and generate color centers in some alkali-halides. These effects have been used for pumping semiconductor lasers[9] and distributed feedback tunable i. r. lasers.[10] The

multi-photon absorption provides a damage mechanism,[11,12] and thus it may determine the damage threshold of the material. This mechanism is especially important in u. v. windows. With the recent development in high power u. v. lasers, practical interest has arisen in the absolute TPA coefficients of the window materials in the u. v. region where published data are quite limited. In harmonic generating crystals, the limited conversion efficiencies have been assigned to nonlinear absorption,[13] or to phase mismatch[14] by different authors. Accurate measurement of the nonlinear absorption coefficients is useful in resolving this issue.

In Sec. II, a brief review of pertinent theories of TPA in solids is presented. The experimental setup and procedure are discussed in Sec. III. In Sec. IV, the results are presented and in Sec. V, our results are compared with calculations based on the Keldysh theory of high frequency tunneling.

II. Theory

In materials with band gap greater than one-photon but smaller than the two-photon energy of an interacting light, it is possible to have absorption by simultaneously absorbing two or more photons from a single laser beam. The two-photon transition rate per unit volume may be obtained by the second order perturbation theory

$$W^{(2)} = \frac{(2\pi)^3}{n_0^2 c^2 \hbar^2} \left(\frac{I}{\hbar}\right)^2 \sum_f |M_{fg}|^2 \, \delta(\omega_{fg} - 2\omega) \, , \tag{1}$$

where

$$M_{fg} = \frac{e^2}{m^2 \omega^2} \sum_i \frac{(\vec{p}_{fi} \cdot \hat{a})(\vec{p}_{ig} \cdot \hat{a})}{\omega_{ig} - \omega} \, ,$$

n_0 is the index of refraction, c is the velocity of light in vacuum, m and e are the mass and charge of the electron, respectively, and I is the intensity of the laser. Summations are extended over final states $|f\rangle$, and intermediate states $|i\rangle$. The initial ground state is denoted by $|g\rangle$. $\hat{a}$ is a unit vector in the direction of the electric field. $\vec{p}_{ij}$ is the matrix element of the momentum operator between the states i and j. $\hbar\omega_{ij}$ is the energy difference between the latter states.

In the standard perturbation approach, the matrix elements and the energy levels [see Eq. (1)] are found from the solutions of the unperturbed Hamiltonian. Another approach to attack the high order transition rates problem was developed by Keldysh,[15] who takes into account the main effect of the electromagnetic field at the first step of the calculations. In this formalism, the transition rate between the Stark-shifted states

$$\psi(\vec{r},t) = U_{\vec{p}(t)}(\vec{r}) \exp\left\{\frac{i}{\hbar}\left[\vec{p}(t)\cdot\vec{r} - \int_0^t \mathcal{E}(\vec{p}(\tau))\, d\tau\right]\right\}, \qquad (2)$$

where

$$\vec{p}(t) = \vec{p} + \frac{e\vec{E}}{\omega} \sin \omega t ,$$

is obtained. This approach is useful since it takes into account all orders of the perturbation expansion. Using this technique, the multi-photon ionization rate in both gases and solids had been calculated by Keldysh,[15] and others.[16] Keldysh's expression for the transition rate reduces to tunneling at low frequencies while at high frequencies the result reduces to multi-photon absorption. In a solid with fundamental energy band gap E_g, using a simple parabolic energy band structure,[15] the multi-photon transition rate per unit volume is given by the Keldysh formula:

$$W = \frac{2}{9\pi}\,\omega\left(\frac{m^*\omega}{\hbar}\right)^{3/2} \Phi\left[\left(2\left\langle\frac{\Delta}{\hbar\omega}+1\right\rangle - 2\frac{\Delta}{\hbar\omega}\right)^{1/2}\right]$$

$$\cdot \exp\left[2\left\langle\frac{\Delta}{\hbar\omega}+1\right\rangle\left(1 - \frac{e^2E^2}{4m^*\omega^2E_g}\right)\right]\left(\frac{e^2E^2}{16m^*\omega^2E_g}\right)^{\left\langle\frac{\Delta}{\hbar\omega}+1\right\rangle}, \qquad (3)$$

where

$$\Delta = E_g + e^2E^2/4m^*\omega^2 .$$

$\Phi(z) = e^{-z^2}\int_0^z e^{y^2}\,dy$ is the Dawson integral. E is the peak field, m^* is the effective reduced mass of the electron and hole pair, $\langle\ \rangle$ means the integer part of the argument.

The complex field dependence of this equation may be simplified in the high frequency limit. The dominant field dependence is then given by

the last factor in the transition rate [Eq. (3)]. The N-photon absorption coefficient γ_N is defined by the expression

$$\gamma_N = \frac{2}{9\pi} N\hbar\omega^2 \left(\frac{3\pi}{n_0}\right)^N \left(\frac{m^*\omega}{\hbar}\right)^{3/2} \phi\left[\left(2N - 2\frac{\Delta}{\hbar\omega}\right)^{1/2}\right]$$

$$\cdot \exp\left[2N\left(1 - \frac{e^2E^2}{4m^{*2}\omega^2E_g}\right)\right]\left(\frac{e^2}{16m^{*2}\omega^2E_g}\right)^N , \qquad (4)$$

which has only a very weak field dependence through Δ. The cross sections may be obtained by transmission versus laser intensity measurements. In the case of one- and two-photon absorbing medium one obtains, with $\gamma_1 = \alpha$ and $\gamma_2 = \beta$, for the transmitted intensity

$$I(\vec{r}, \ell, t) = (1 - R)^2 I(\vec{r}, 0, t)\, e^{-\alpha\ell}/\{1 + \beta(1 - R)I(\vec{r}, 0, t)(1 - e^{-\alpha\ell})/\alpha\} , \qquad (5)$$

where ℓ is the length of the sample, and R is the reflectivity.[17] Multiple reflections are neglected in the derivation of the above equation.

Since we wish to compare, in this paper, multi-photon transitions of different order, we have used the Keldysh theory for estimations of multi-photon cross sections. Because this theory is based on a very simplified band structure, the present calculations are not expected to be accurate. Satisfactory agreement, however, was achieved between the dispersion of β measured here and the Keldysh's expression, using one adjustable parameter.

The TPA coefficient may also be expressed in terms of the imaginary part of the third order nonlinear susceptibility tensor

$\chi^{(3)}_{ijkl}(-\omega, \omega, \omega, -\omega)$. For cubic crystals, with 432, $\bar{4}3m$ or $m\bar{3}m$ symmetry and a single laser frequency, $\chi^{(3)}$ has only three independent elements.[18] These elements may be obtained by the measurement of the TPA cross section in three different polarization conditions. First, it is convenient to measure the diagonal element χ''_{xxxx} according to the relation

$$\beta = (32\,\pi^2\,\omega/n_0^2c^2)\,[3\,\chi''_{xxxx}(-\omega, \omega, \omega, -\omega)]\ , \qquad (6)$$

which is derived in the Appendix. Here ω is the laser angular frequency, c is the speed of light in vacuum, n_0 is the index of refraction. We are using the Maker and Terhune convention,[19] with a degeneracy factor 3, because there are three distinct permutations of the positive and negative frequency arguments. As shown in the Appendix, for linearly polarized light in the $[1, 1, 0]$ direction, the TPA coefficient is

$$\beta = (16\pi^2\omega/n_0^2c^2)[3\,\chi''_{xxxx}(-\omega, \omega, \omega, -\omega) + 6\,\chi''_{xxyy}(-\omega, \omega, \omega, -\omega) + 3\,\chi''_{xyyx}(-\omega, \omega, \omega, -\omega)]\ . \qquad (7)$$

And for circularly polarized light, with light propagating along $[0, 0, 1]$,

$$\beta = (16\pi^2\omega/n_0^2c^2)[3\chi''_{xxxx}(-\omega, \omega, \omega, -\omega) + 6\,\chi''_{xxyy}(-\omega, \omega, \omega, -\omega) - 3\,\chi''_{xyyx}(-\omega, \omega, \omega, -\omega)]\ . \qquad (8)$$

III. Experimental Setup and Procedure

The Nd:YAG laser oscillator-amplifier system is described in Ref. 17. Passive mode-locking is employed with a spark-triggered electro-optical shutter to select a single pulse having energy up to 10 mJ. The beam profile was measured carefully. It is Gaussian both in space and time. The pulses have an average duration of 30 ps at full width half maximum. The fundamental laser frequency is doubled by a temperature tuned 90° phase matched CDA crystal (see Fig. 1a). The energy conversion efficiency at 100 MW input is 50%. The third harmonic (355 nm) is generated by mixing the fundamental and the second harmonic frequencies in an angle tuned KDP crystal. The energy profile of the beam is monitored by photo-diode array (AR), and fitted with a Gaussian curve with a $1/e$ radius $d = 0.78$ mm. The fourth harmonic (266 nm) is generated by frequency doubling the second harmonic in a temperature tuned 90° phase matched ADP crystal. The beam is again fitted with a Gaussian of radius $d = 0.68$ mm. The overall energy conversion efficiency to 355 nm is 10%, to 266 nm 15%. Unwanted frequencies are filtered out by color filters as shown in Fig. 1a, or by a dispersive prism used at minimum deviation in order not to distort the beam.

In order to determine the TPA cross section, the energy transmission coefficient through the sample is measured. For a Gaussian beam with a maximum on-axis input intensity I_p, we may write for the transmitted intensity

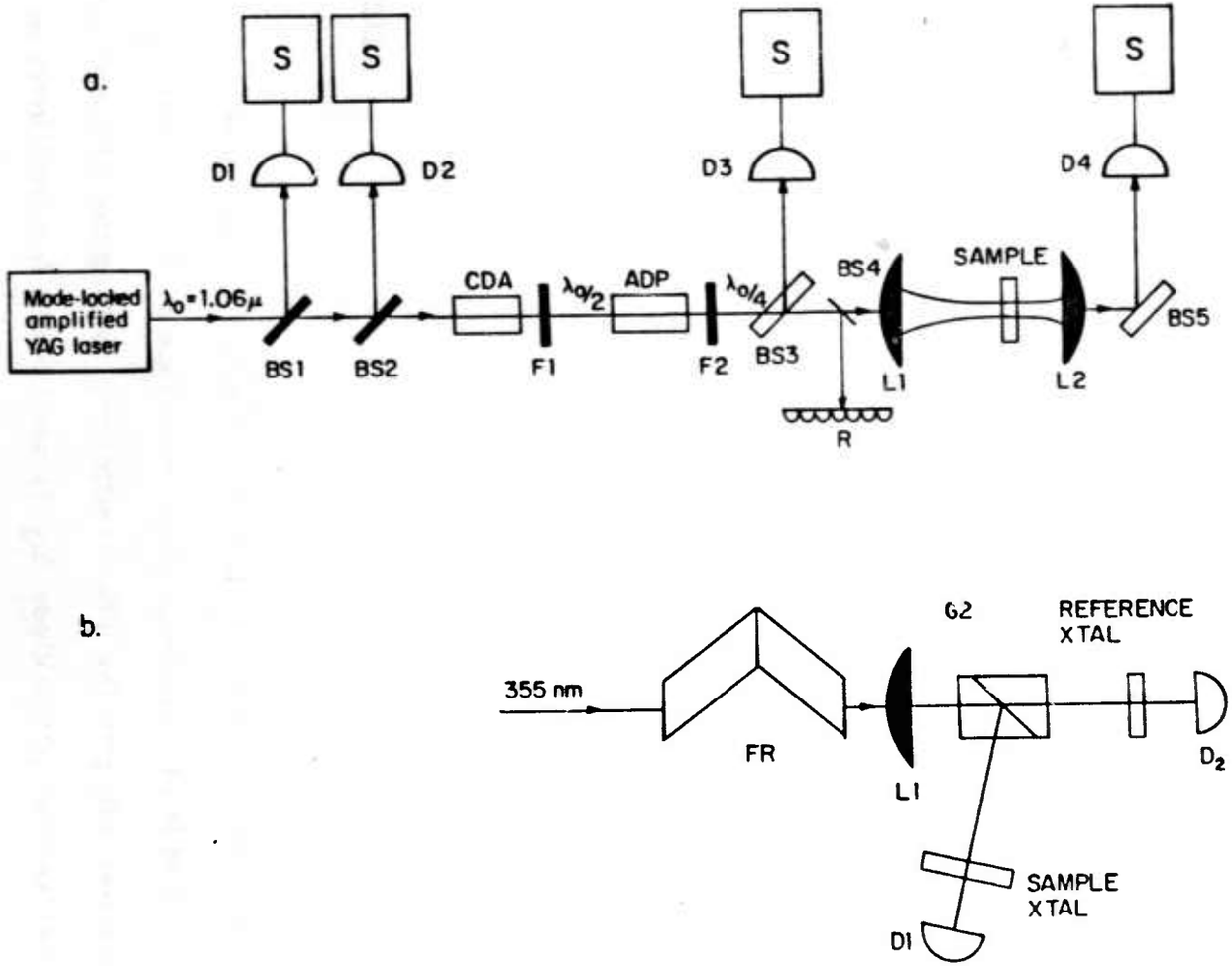

Figure 1. a. Schematic diagram of the absolute TPA experimental setup at 266 nm. BS: Fused silica beam splitters, D: Vacuum photo-diodes, L: Quartz lenses, F: Color filters (Corning Glass 1-56, 7-54), AR: Linear photo-diode array, S: Represents a scope or electronic integrator.

b. Schematic diagram of the relative measurement setup. G: Glan prisms, FR: Double Fresnel rhomb, L: Lens, D: Photo-diodes.

$$I(r,\ell,t) = \frac{I_p(1-R)^2 \exp[-(r/d)^2 - (t/\tau)^2]\exp(-\alpha\ell)}{1+\beta I_p(1-R)\exp[-(r/d)^2 - (t/\tau)^2][1-\exp(-\alpha\ell)]} \quad , \tag{9}$$

while the energy transmission coefficient is given by:

$$T = \frac{\mathcal{E}^{out}}{\mathcal{E}^{in}} = \frac{2\pi \int_0^\infty r\,dr \int_{-\infty}^{\infty} I(r,\ell,t)\,dt}{I_p \pi^{3/2} d^2 \tau}$$

$$= 2\,\frac{\alpha \exp(-\alpha\ell)(1-R)}{\pi^{1/2}\beta I_p[1-\exp(-\alpha\ell)]} \int_0^\infty \ell n\left\{1 + \frac{\beta}{\alpha} I_p(1-R)[1-\exp(-\alpha\ell)] \cdot \exp(-x^2)\right\} dx \quad . \tag{10}$$

At low intensity, we find:

$$\lim_{I_p \to 0} T = (1-R)^2 \quad , \tag{11}$$

$$\lim_{I_p \to 0} d\,\frac{1}{T}\,/dI_p = \beta\ell/[2^{3/2}(1-R)] \quad . \tag{12}$$

The approximation is good for $I_p(1-R)(1-e^{-\alpha\ell})\beta/\alpha < 1$ and $\alpha \ll 1$, which is satisfied in all samples. Thus, the slope of $1/T$ versus I_p at low intensities will give the TPA coefficient. During the TPA measurement a planar vacuum photo-diode D_1 is used with a fast oscilloscope to make sure that the beam is a single pulse. The fluctuation in the pulse area and duration is taken into account by monitoring the energies of each pulse at 1.06 μm and its harmonics.[20] A fundamental Gaussian pulse

$$I_0(r,t) = I_p \exp[-(r/d)^2-(t/\tau)^2] \quad , \tag{13}$$

generates a second harmonic

$$I_{2\omega}(r,t) = g_{2\omega} I_p^2 \exp[-2(r/d)^2-2(t/\tau)^2] \quad .$$

Here $g_{2\omega}$ is the conversion efficiency. The energy of the fundamental is $\mathcal{E}_0 = \pi^{1/2} I_p \tau A$ where $A = \pi d^2$. The second harmonic energy is $\mathcal{E}_{2\omega} = g_{2\omega} \pi^{1/2} I_p^2 (\tau A)_2$, where $(\tau A)_2 = \tau A \cdot 2^{-3/2}$. Similarly, the third and fourth harmonics have $\mathcal{E}_{3\omega} = g_{3\omega} \pi^{1/2} I_p^3 (\tau A)_3$, $\mathcal{E}_{4\omega} = g_{4\omega} \pi^{1/2} I_p^4 (\tau A)_4$, with $(\tau A)_3 = \tau A \cdot 3^{-3/2}$, $(\tau A)_4 = \tau A \cdot 8^{-1}$. For constant conversion efficiency, we may write:

$$\frac{\mathcal{E}_0^2}{\mathcal{E}_{2\omega}} \propto \left(\frac{\mathcal{E}_0^3}{\mathcal{E}_{3\omega}}\right)^{1/2} \propto \left(\frac{\mathcal{E}_0^4}{\mathcal{E}_{4\omega}}\right)^{1/3} \propto \tau A \quad . \tag{14}$$

However, as is shown in Fig. 2, the experimental ratio of $(\mathcal{E}_0^3/\mathcal{E}_{3\omega})^{1/2}/(\mathcal{E}_0^2/\mathcal{E}_{2\omega})$ depends somewhat on the input intensity. This deviation from a horizontal line indicates that some saturation effects in the harmonics conversion efficiency and/or a change in the laser pulse shape occurs as the laser intensity is enhanced by increasing the voltage on the laser amplifiers. For a constant voltage, however, the ratio $(\mathcal{E}_0^3/\mathcal{E}_{3\omega})^{1/2}/(\mathcal{E}_0^2/\mathcal{E}_{2\omega})$ is nearly constant while the intensity is varied with attenuators. The latter effect and the narrowly distributed data shown in Fig. 2 show that the main fluctuation is coming from the fundamental beam and that τA technique provides a good correction from pulse to pulse at the same nominal intensity. In Fig. 3, we show a set of data plotted with and

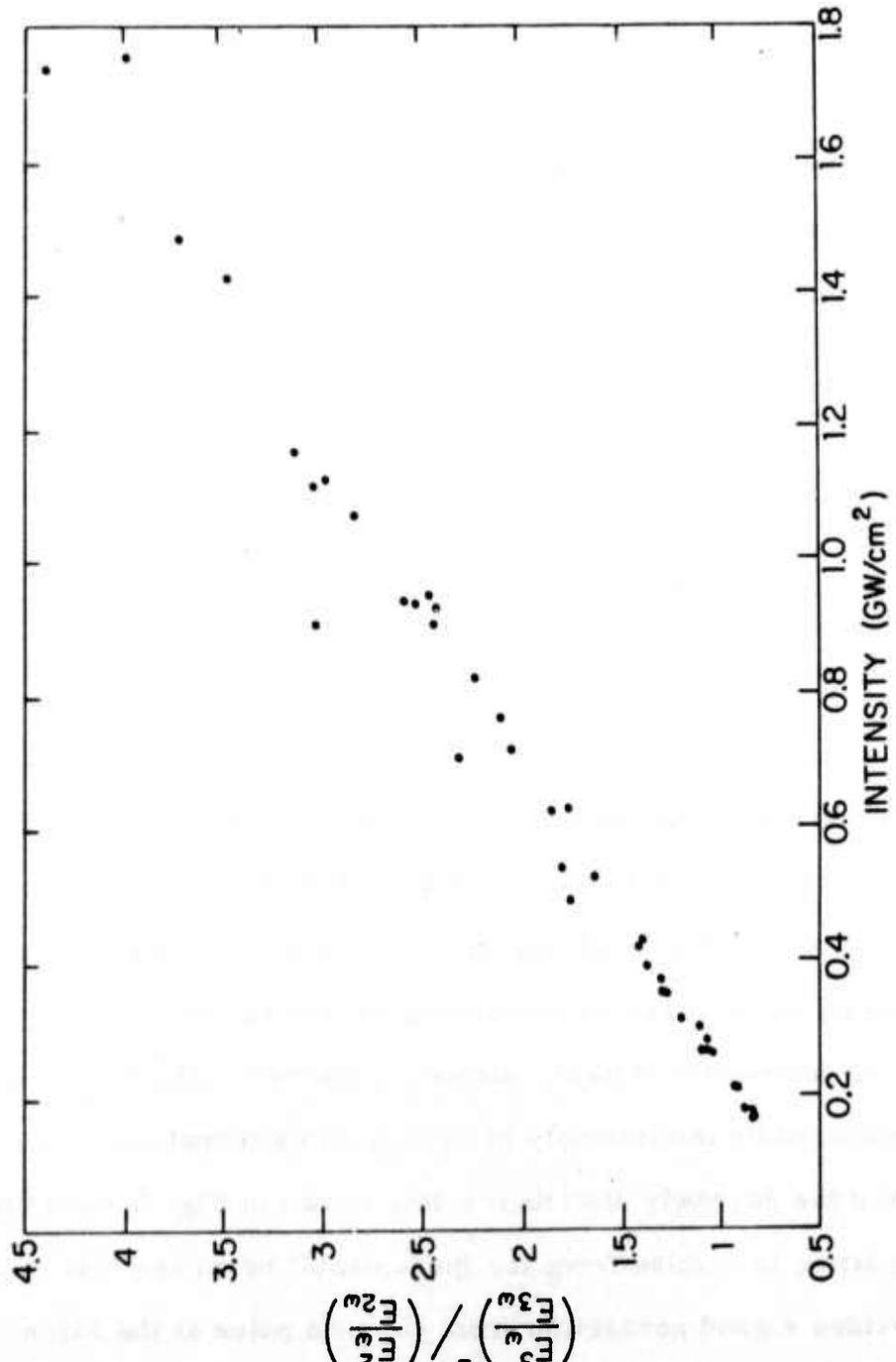

Figure 2. The ratio of τA, found by using the third and second harmonic beams is plotted as a function of the fundamental input intensity. The input intensity is corrected using $(\tau A)_2$ obtained by the second harmonic beam.

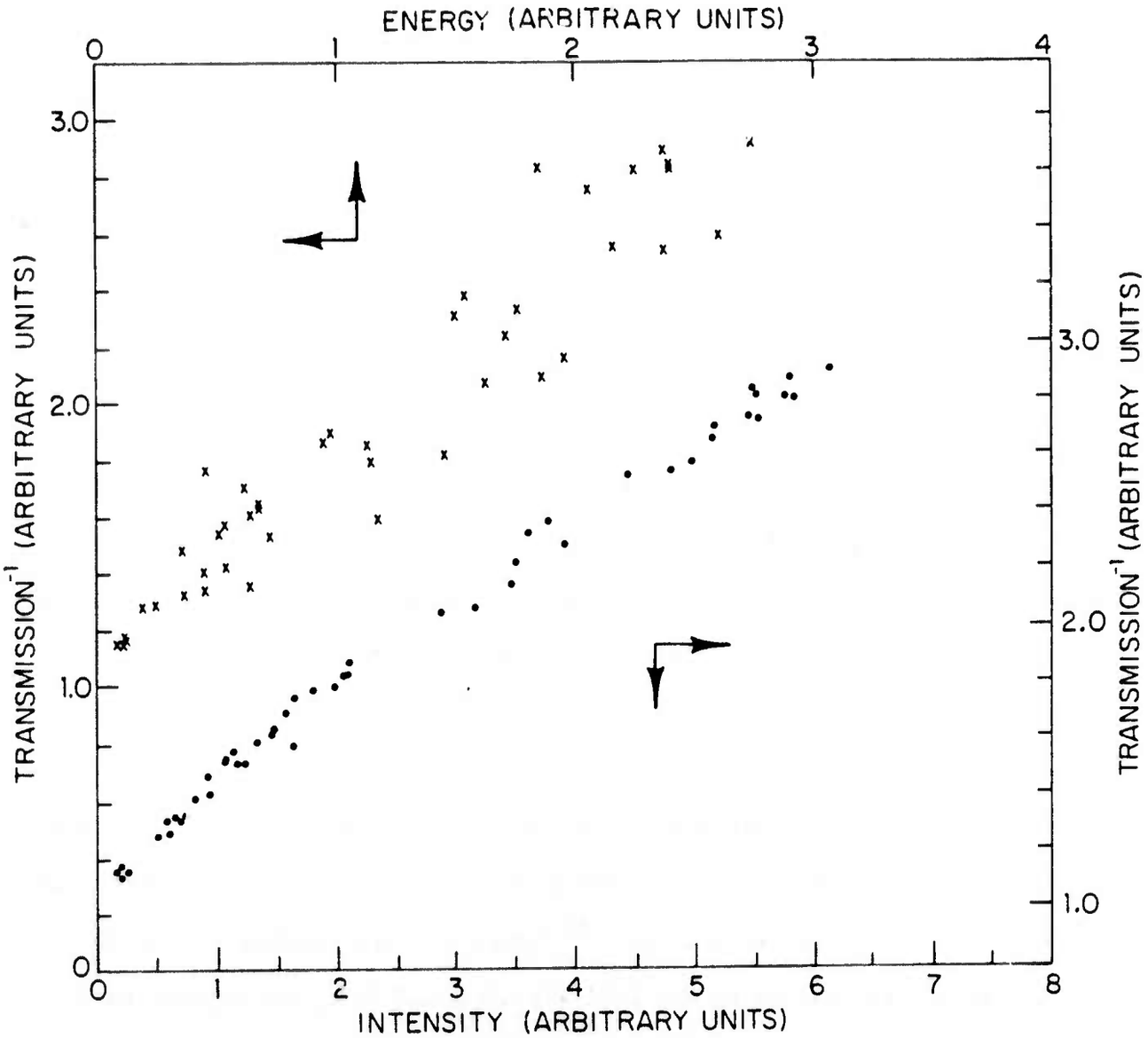

Figure 3. Plot of the reciprocal energy transmission coefficient vs. intensity (dots, analyzed with τA technique) or energy (cross, analyzed without τA). Note the two sets of scales.

without a correction by the τA technique. This data clearly demonstrate the above statement.

The τA correction technique may introduce systematic error at high amplifier voltage setting due to saturation. In the intensity range of the TPA experiment performed here, we observed that the average τA increases by 50% at the peak power used (100 MW) using $(\tau A)_2$ obtained from the beam at 2ω for intensity corrections. We note that the harmonic signal used for obtaining the various τA were obtained from the same harmonic beams utilized in the TPA experiments. The generation of 3ω which is done in an angle tuned crystal, critically depends on the preceding second harmonic generation step which is done in a 90° CDA crystal. Because of the nature of the mixing process, it is clear that the value of τA obtained from the energy of the beam at 2ω is more reliable than the value obtained from the beam at 3ω. Therefore, we analyzed our data using $(\tau A)_2$ for the correction.

The laser energy is measured with the diode D_3 which is calibrated with respect to a thermopile and a pyroelectric energy meter. The outputs of all photo-diodes were recorded by oscillograms or by homemade peak detect-amplifier-holding circuits[21] which give the reading on digital displays. For analyzing the TPA experimental data, the approximate value of β is found using Eq. (12) and then a set of curves are generated using Eq. (10) with different values of β close to the approximate value. The TPA coefficient β is then chosen by the best fit curve as represented by the line in Fig. 4a.

Because the TPA cross sections are rather small, a lens (see Fig. 1a) is used to increase the effective nonlinear absorption by increasing the

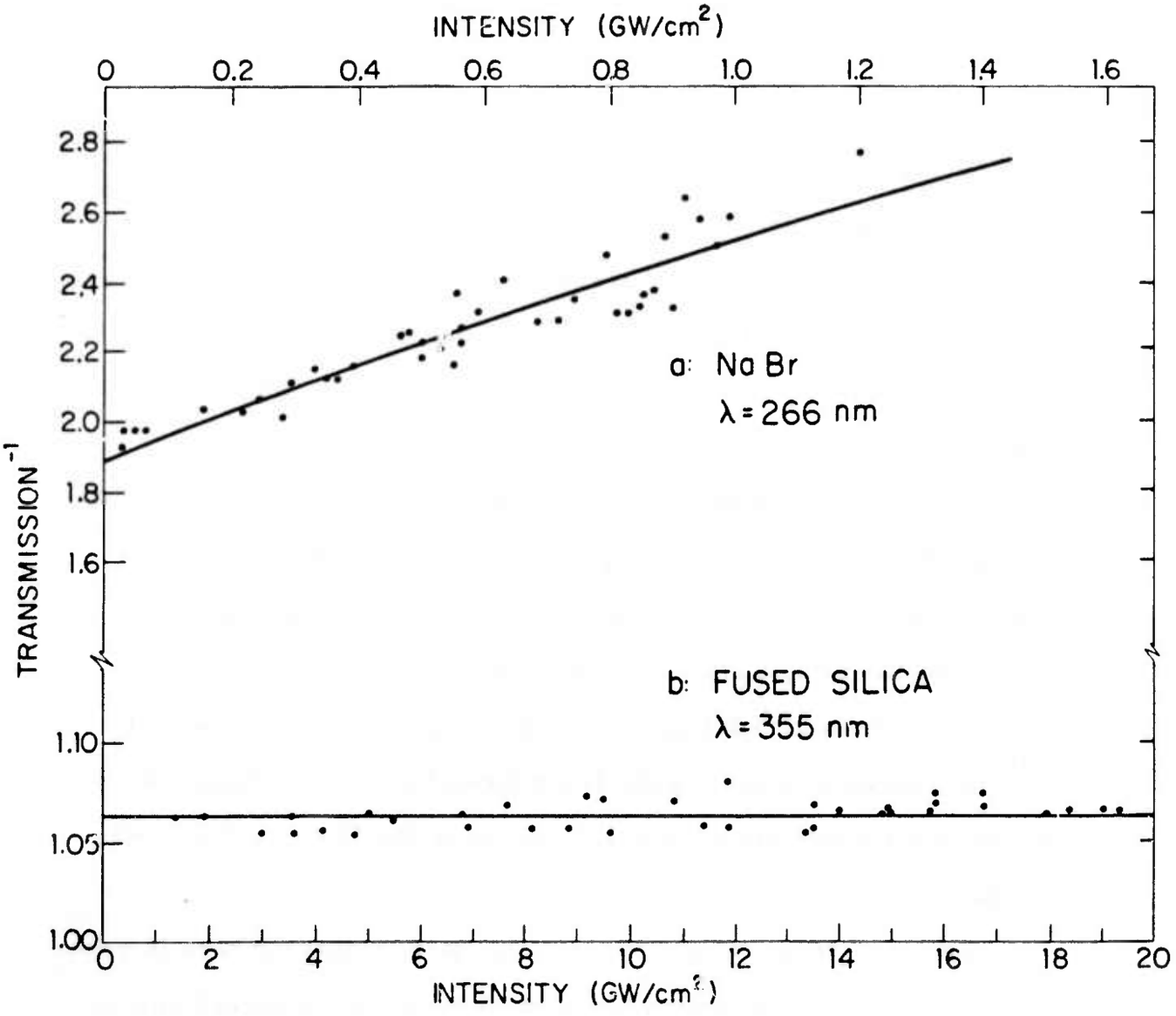

Figure 4. a. Plot of the reciprocal energy transmission vs. maximum incident intensity for NaBr. Sample thickness is 0.74 cm, laser electric field is in the [1, 0, 0] direction. The drawn theoretical line is generated using Eq. (10) with $\beta = 2.5 \times 10^{-3}$ cm/MW.

b. Typical plot of inverse energy transmission vs. the input intensity for materials with band gap greater than $2\hbar\omega$. Note the differences in the horizontal and vertical scales in parts a and b.

intensity of the beam at the sample. Since the geometry is critical in the determination of β, the focal length of this lens (L1) is measured carefully. This is done at each wavelength used because the dispersion is quite large in the spectral region of the measurement.

The samples are put behind the focal point of the lens (L1) to avoid damage caused by the effect of self-focusing. Reflections from the back surface of the beam splitter BS 3 (Fig. 1a) and the front surface of BS 5 are used to avoid error introduced by TPA in the beam splitters themselves.

In order to eliminate any possible accumulated effects on the TPA measurement (such as F-center generation), each transmission data point was performed at a fresh site in the sample. This was done by translating the sample after each laser shot.

The circularly polarized beam used to probe the anisotropy of $\chi^{(3)}$ is generated by passing the beam through a Fresnel rhomb, with proper beam polarization. The circularity is checked by a Glan prism analyser.

The uncertainty of the relative value of β measured here is quite small. The main contribution to this uncertainty is the uncertainty in the experimental value of τA. On the average this introduces an uncertainty of $\pm$ 15%. The scattering of the data points gives on the average another $\pm$ 10%. The individual uncertainty for each sample is lited in Tables 1 and 2. The systematic error in the absolute determination of β, an uncertainty which should be added to the previous one, is $\pm$ 7% in absolute energy calibration, $\pm$ 28% in the average value of τA at low intensity, and $\pm$ 8% caused by the $\pm$ 1.5 mm uncertainty in the

determination of the focal length of the lens (L1). Thus, the absolute uncertainty sums up to ± 43%.

The experimental setup for the relative measurement with the two-channel normalization technique[6] is shown in Fig. 1b. A double Fresnel rhomb is used here to vary in an efficient way the intensities going to the sample and reference channels. The ratio of the energy transmitted through the sample and the reference is given by

$$\rho = \frac{\mathcal{E}_s}{\mathcal{E}_r} = \frac{a_s e^{-a_s \ell_s}(1-R_s)}{1-e^{-a_s \ell_s}} \cdot \frac{1-e^{-a_r \ell_r}}{a_r\, e^{-a_r \ell_r}\,(1-R_r)} \cdot \frac{\beta_r}{\beta_s}$$

$$\cdot \frac{\int_0^\infty \ell n\left[1 + \frac{\beta_s}{a_s} I_s (1-R_s)(1-e^{-a_s \ell_s})\, e^{-x^2}\right] dx}{\int_0^\infty \ell n\left[1 + \frac{\beta_r}{a_r} I_r\, (1-R_r)(1-e^{-a_r \ell_r})\, e^{-x^2}\right] dx} \cdot \qquad (15)$$

At proper filter factor, $F = I_s/I_r$, the integrands in Eq. (15) are equal and the ratio ρ will be independent of intensity. We have then

$$\frac{\beta_s}{\beta_r} = \frac{a_s(1-R_r)(1-e^{-a_r \ell_r})}{F\; a_r (1-R_s)(1-e^{-a_s \ell_s})} \cdot \qquad (16)$$

To check the reliability of the setup for this experiment we used identical samples of KI as sample and reference. Fig. 5 shows clearly that the expected value of $F = 1$ was obtained.

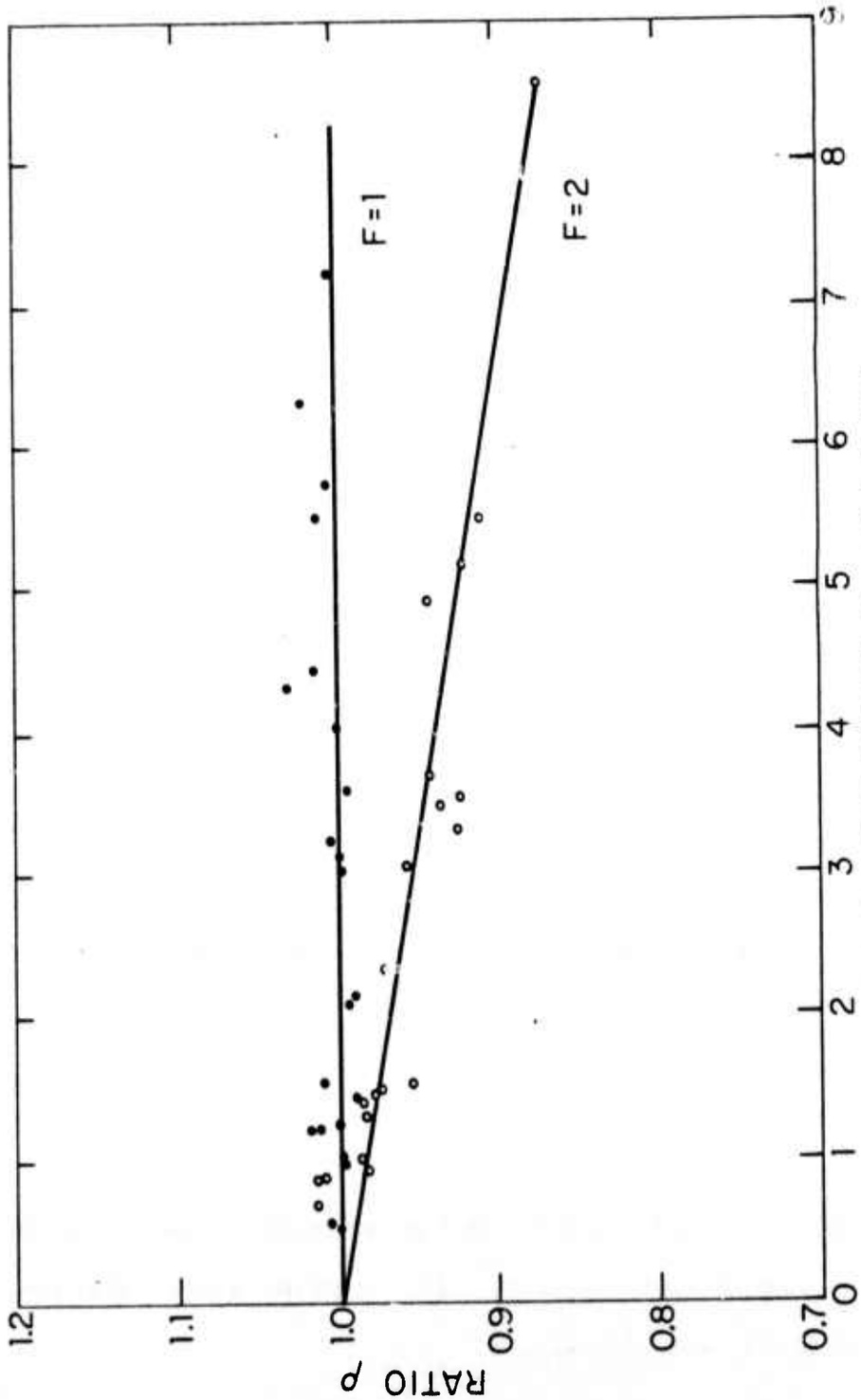

Figure 5. The ratio of energy transmitted through the sample and the reference vs. the energy transmitted through the reference in the relative measurement. Data were taken with KI vs. KI with different filter factors F = 1 (dots), F = 2 (circles).

IV. Experimental Results

At 355 nm, we measured the absolute TPA coefficients in three alkali-halides, as well as in KDP and 10 other harmonic generating crystals. These are all listed in Table 1. Upper limits for β in the commonly used u.v. window materials, Sapphire and fused silica, with band gaps greater than $2\hbar\omega$ (7.02 eV) are also tabulated. For the materials measured with band gaps greater than $2\hbar\omega$, the transmission T is practically constant to intensity up to 20 GW/cm^2. Fig. 4b shows a typical transmission plot for material with large band gap. Higher beam intensities could not be used due to the onset of surface damage.

The anisotropy of the TPA was measured in RbI. Linear polarized light in the [1,,0,0] and [1,1,0] directions show the same value of β. According to Eqs. (6) and (7), this suggests the isotropy condition

$$2\chi''_{xxyy} + \chi''_{xyyx} = \chi''_{xxxx} \quad . \tag{17}$$

The circularly polarized beam showed a smaller TPA. The ratio for the three elements of $\chi^{(3)}$ calculated from Eqs. (6-8) are $\chi''_{xxxx} : \chi''_{xxyy} : \chi''_{xyyx} = 1 : 0.455 : 0.09$, with the absolute value $\chi''_{xxxx} = 2.72 \times 10^{-13}$ cm^3/erg. Anisotropy of the tetragonal crystal CD^*A was also observed. The value of β with the beam polarized in the x-y plane is larger, by a factor 1.8, than that obtained when the E-field is parallel to z axis. Although some second harmonic generation may occur in the former case, this radiation is not phase matched. The power conversion efficiency at an input intensity of 10 GW/cm^2 is estimated to be 10^{-5} and therefore the measured value of β is not affected.

TABLE 2

Material	E_g (eV)[a]	Surface Normal $\vec{N}$[b]	$\vec{E}/\lvert\vec{E}\rvert$[c]	P_{cr} (KW)[a]	ℓ(cm)	β(cm/MW)[d]	m^*/m[e]	n[a]
NaCℓ	6.36	[1 0 0]	[0 0 1]	16	0.74	3.5×10^{-3} ± 25%	5.3×10^{-3}	1.637
NaCℓ	6.36	[1 0 0]	[0 1 1]	16	0.74	3.6×10^{-3} ± 30%		
NaBr	7.7	[1 0 0]	[0 0 1]	8	0.74	2.5×10^{-3} ± 15%	1.03×10^{-2}	1.803
KCℓ	6.52	[1 0 0]	[0 0 1]	20	0.74	1.7×10^{-3} ± 20%	2.46×10^{-2}	1.571
KCℓ (F-centers)		[1 0 0]	[0 0 1]	20	0.74	1.8×10^{-3} ± 30%		
KCℓ	6.52	[1 0 0]	[0 0 1]	20	2.10	2.7×10^{-3} ± 30%		
KBr	6.00	[1 0 0]	[0 0 1]	4.5	0.74	2.0×10^{-3} ± 30%	1.46×10^{-2}	1.76
KI	5.06	[1 0 0]	[0 0 1]	6	0.47	3.75×10^{-3} ± 30%	4.8×10^{-3}	1.938
RbCℓ	7.29	[1 0 0]	[0 0 1]		0.60	1.02×10^{-3} ± 15%	4.54×10^{-2}	1.576
RbCℓ	7.29	[1 0 0]	[0 0 1]		1.91	1.26×10^{-3} ± 30%		
RbBr	5.40	[1 0 0]	[0 0 1]		1.0	2.18×10^{-3} ± 20%	2.02×10^{-2}	1.686
RbI	5.04	[1 0 0]	[0 0 1]		1.0	2.49×10^{-3} ± 20%	1.15×10^{-2}	1.917
$CaCO_3$	5.88				0.43	2.4×10^{-4} ± 30%	1.11	1.750 (n_o) 1.526 (n_e)
KDP	6.95	1.06μ→0.53μ cut		67	0.57	2.7×10^{-4} ± 30%	0.72	1.560 (n_o) 1.510 (n_e)
ADP	6.81				0.5	2.4×10^{-4} ± 30%	0.90	1.580 (n_o) 1.527 (n_e)
$Aℓ_2O_3$	7.3	C-axis			0.5	2.7×10^{-4} ± 30%	0.353	1.833 (n_o)
$Aℓ_2O_3$	7.3	⊥C-axis			0.5	2.7×10^{-4} ± 30%		
SiO_2 (fused silica)	7.8			70	0.64	4.5×10^{-5}	50	
SiO_2 (Quartz)	7.8	⁻C-axis			1.2	4.5×10^{-5}	50	
LiF	11.6	[1 0 0]	[0 0 1]	73	0.47	$<2\times10^{-5}$		1.415
CaF_2	10.0	[1 0 0]	[0 0 1]	60	0.47	$<2\times10^{-5}$		

Table 1. The TPA experimental results at 355 nm.

a. Energy gand gap (E_g), self-focusing critical power (P_{cr}), and refractive index (n) are given whenever available.
b. All measurements were done normal to the crystal surface.
c. $\vec{E}/\lvert\vec{E}\rvert$ is the direction of the laser polarization.
d. The total uncertainty in β is the sum of the relative uncertainty (listed in the table for each material) and the systematic uncertainty of the experiment estimated to be ± 43%.

In addition to the absolute determination of β we measured the relative values of β in RbBr versus KI and RbI versus KI as described above. The ratios obtained $\beta(RbBr)/\beta(KI) = 0.305$ and $\beta(RbI)/\beta(KI) = 0.668$ agree within 10% with the absolute values in Table 1. This agreement between the two measurements suggests that the uncertainty estimation presented in Sec. III is quite conservative.

At 266 nm, we measured the TPA in 8 alkali-halides with band gap less than $2\hbar\omega$ (9.36 eV), and in KDP, ADP, Calcite, Sapphire and SiO_2. The window materials LiF and CaF_2 in which no TPA is expected are also measured. The measured values are listed in Table 2. For alkali-halides the β values measured are of the order of 10^{-3} cm/MW, while for KDP, ADP, calcite and sapphire, they are of the order of 10^{-4} cm/MW. For the materials with band gaps greater than $2\hbar\omega$, an upper limit for β is given. It is important to note that fused silica and quartz have quite small TPA at this wavelength.

Fluorescence is observed in all the alkali-halides along the path of the beam.[22,23] Coloring can be seen with the bare eye after a few shots. In KCl the absorption of a monitoring beam at 532 nm by the color track is observed and can be explained by the spectral position of the absorption band of the F-center.[24] The physical process involves the generation of electron-hole pairs by two-photon excitation. The pairs recombine to form excitons with the emission of fluorescent light. The exciton energy is given up to form V_K and F-centers.[25] We have found that the F-centers, generated by several hundred shots of the laser at the same site of the crystal, did not influence the transmission of the crystal at the laser frequency after they had relaxed in few seconds.

TABLE 1

Material	E_g (eV)[a]	Surface Normal $\vec{N}$[b]	$\vec{E}/\lvert\vec{E}\rvert$[c]	P_{cr} (KW)[a]	ℓ(cm)	β(cm/MW)[d]	n[a]
KI	5.06	[1 0 0]	[0 0 1]	11	0.47	7.29×10^{-3} ± 20%	1.765
RbBr	5.40	[1 0 0]	[0 0 1]		1.0	2.43×10^{-3} ± 20%	1.600
RbI	5.04	[1 0 0]	[0 0 1]		1.0	5.08×10^{-3} ± 15%	1.731
RbI	5.04	[1 0 0]	[0 1 1]		1.0	5.08×10^{-3} ± 25%	
RbI	5.04	[1 0 0]	Circularly polarized		1.0	4.62×10^{-3} ± 20%	
ADA		45° z cut	z-axis		1.6	3.53×10^{-5} ± 30%	
ADP	6.81	45° z cut	z-axis		2.0	6.8×10^{-6} ± 35%	1.548 (n_o) 1.499 (n_e)
CDA		45° z cut	⊥z-axis		1.4	8.02×10^{-5} ± 30%	1.60 (n_o) 1.57 (n_e)
CD*A		45° z cut	z-axis		1.4	5.12×10^{-5} ± 30%	1.59 (n_o) 1.57 (n_e)
CD*A		45° z cut	z-axis		1.15	2.81×10^{-5} ± 35%	
KDA		45° z cut	z-axis		1.0	4.84×10^{-5} ± 30%	1.59 (n_o) 1.54 (n_e)
KD*A		45° z cut	z-axis		1.0	2.66×10^{-5} ± 35%	
KDP	6.95	45° z cut	z-axis		1.0	5.9×10^{-6} ± 35%	1.531 (n_o) 1.486 (n_e)
KD*P		45° z cut	z-axis		1.0	5.4×10^{-6} ± 35%	1.53 (n_o) 1.49 (n_e)
RDA		45° z cut	z-axis		1.25	4.99×10^{-5} ± 30%	1.60 (n_o) 1.55 (n_e)
RDP		45° z cut	z-axis		1.0	$<5.9 \times 10^{-6}$	1.53 (n_o) 1.50 (n_e)
A_2O_3	7.3	C-axis			0.5	$<1.6 \times 10^{-6}$	1.796 (n_o)
SiO_2 (fused silica)	7.8				0.64	$<1.25 \times 10^{-6}$	1.476

Table 2. The TPA experimental results at 266 nm.

a. Energy band gap (E_g), self-focusing critical power (P_{cr}), and refractive index (n) are given whenever available.
b. All measurements were done normal to the crystal surface.
c. $\vec{E}/\lvert\vec{E}\rvert$ is the direction of the laser polarization.
d. The total uncertainty in β is the sum of the relative uncertainty (listed in the table for each material) and the systematic uncertainty of the experiment estimated to be ± 43%.
e. m^*/m is the ratio of the effective mass fitted with the Keldysh formula to the observed value of β and the mass of the free electron.

Since the power used in the TPA experiment is much higher than the critical power for self-focusing,[12,26] it is important to look for any change in beam size due to self-focusing. The checks have been done with different sample thickness, also by observing the stable color track formed in a U-center doped KCl under microscope. An attempt was made to record a single shot beam profile in three dimensions by the TPA generated color centers in KCl,[27] but the coloring effect is not strong enough to be observed after a single shot. No evidence of self-focusing has been observed so far, in spite of predictions based on critical power values for self-focusing extrapolated[26] by the scaling factor ω^{-2} from $\lambda = 1.06\,\mu m$ measurements. Since the measurements were done with $2\hbar\omega$ close to the energy gap, the latter extrapolation might be incorrect because of the positive or negative two-photon resonant contributions to the nonlinear refractive index n_2. In addition, the TPA effect which consumes energy from the peak intensity location of the beam competes with the self-focusing process.

Our values of β are about a factor 5 smaller than those obtained more than a decade ago by Fröhlich and Park.[28,29] With the less well controlled beams, nominal values for the intensity are probably considerably lower than the actual intensity in hot spots due to spatial and temporal fluctuations. This could explain their systematically high value of β. A more recent measurement of TPA coefficient $\beta = 2.36 \times 10^{-3}$ cm/MW, by Mollenauer et al.,[27] in KCl is more in line with our data. Reintjes[30] has very recently reported very low values of the TPA coefficients in ADP and deuterated KD^*P. His value for KD^*P $\beta = (2.7 \pm 0.7) \times 10^{-5}$ cm/MW is an order of magnitude lower than our value for the undeuterated KDP. His value for ADP $\beta = (1.1 \pm 0.3) \times 10^{-4}$

cm/MW is a factor of 2.2 lower than ours. The large deviation of the results in the two latter crystals may be explained by differences in impurity concentration in the sample used. It is interesting to note that for the alkali-halides, we measured at both u.v. frequencies, the TPA coefficients at 355 nm are of the same order but somewhat larger than those at 266 nm.

V. Comparison with the Keldysh Theory

The magnitudes for 4-photon, 3-photon, and 2-photon absorption coefficients of NaCl derived from the Keldysh theory [Eq. (4)] are plotted as a function of photon energy in Fig. 6. For a fixed N, γ_N goes through a very shallow maximum as a function of photon energy. The maximum occurs at an energy just before the next lower order photon process becomes possible. The band gap dependence and the effective mass dependence of γ_2, which represent the material dependence in the Keldysh theory, are shown in Fig. 7.

The observed values of β in Table 2 with the known band gap for each material can all be fitted with the Keldysh theory, by adjusting m^* in each case. These adjusted values of m^* are listed in Table 2. It should not be expected that these values correspond to those determined by transport properties from carriers near the bottom of the conduction band. In fact, m^* in the Keldysh theory is largely a measure for the average strength of the dipole matrix element.

Using the m^* found at 266 nm for KI, RbBr and RbI, the frequency dependence of β in each of these materials was calculated. The results are plotted in Fig. 8, along with the experimental points. It is interesting to see that the Keldysh theory does predict a decrease of β with increasing photon energy in qualitative agreement with the experimental trend.

The effect of multi-photon absorption on breakdown can also be calculated by the Keldysh formula. In order to compare this model with the experimental data observed by Smith et al.,[12,31] we calculated the threshold electric field needed to generate enough free electrons by

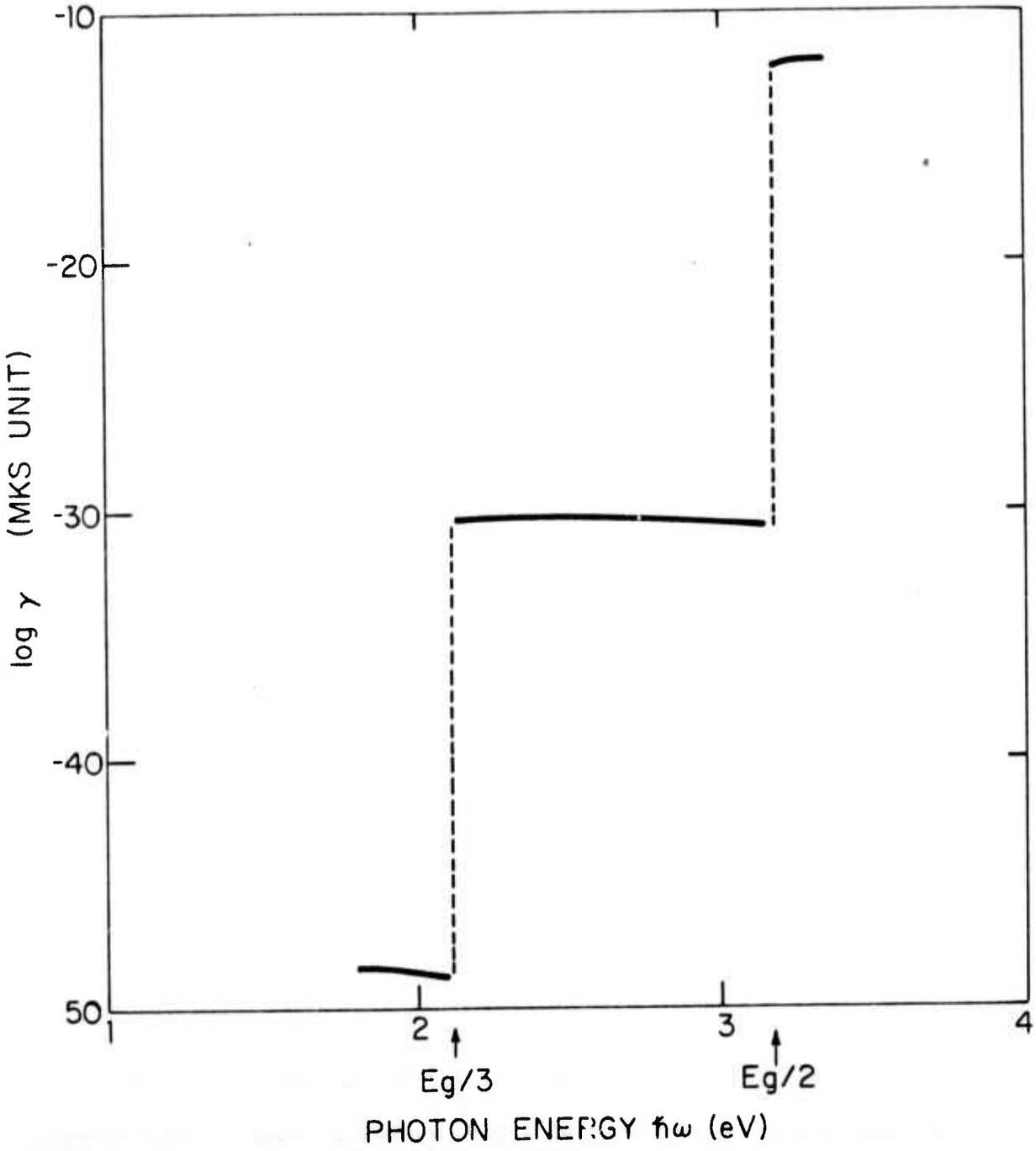

Figure 6. Log of the multi-photon absorption coefficients in NaCl as given by the Keldysh formula vs. photon energy ($m^*/m = 1$ was used). The steps indicate transitions from 4- to 3- and to 2-photon process. The arrows indicate the photon energy as fraction of the energy band gap, E_g.

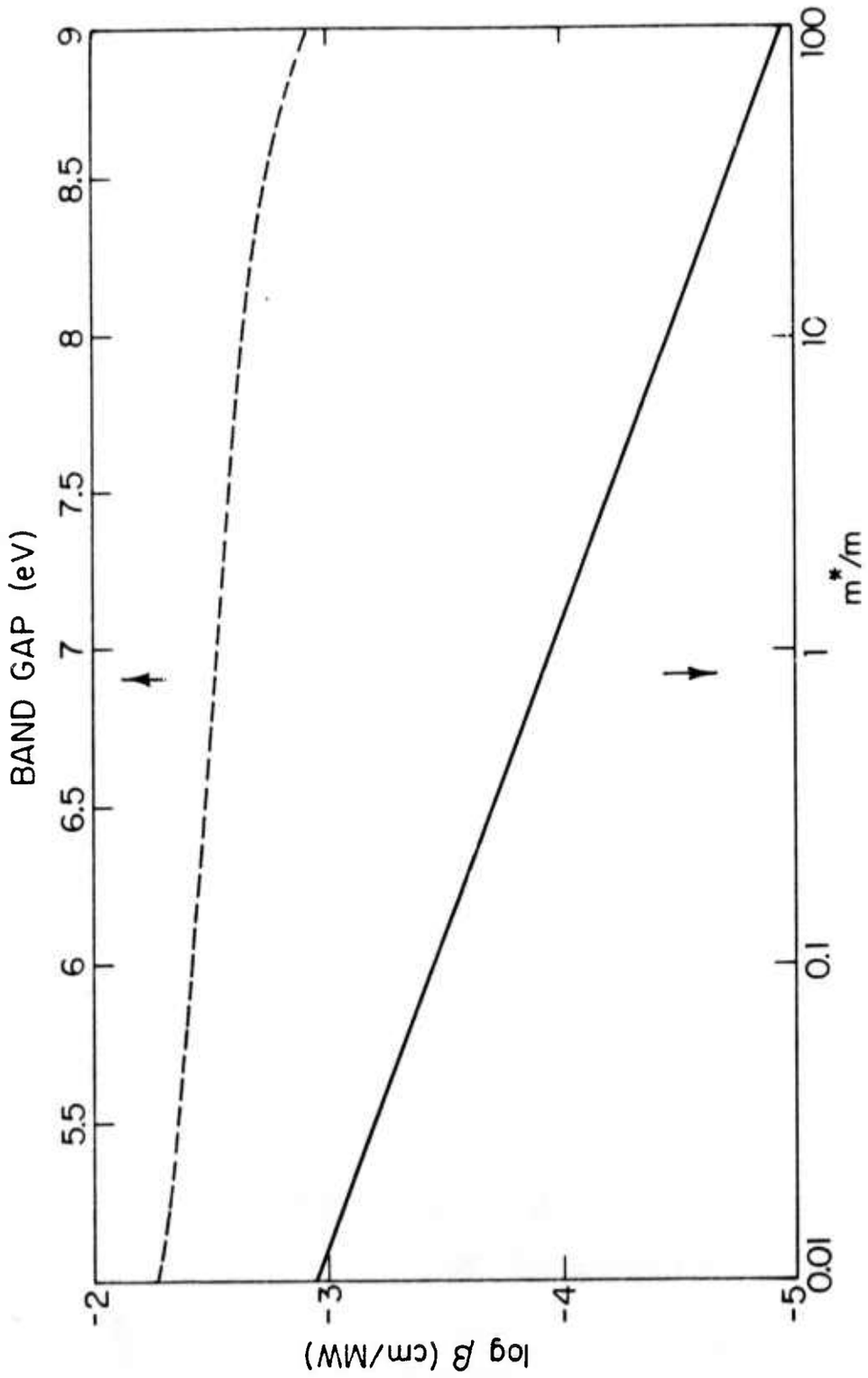

Figure 7. Theoretical value of γ_2 vs. the effective mass (dashed curve) and vs. the band gap (continuous line). The parameters used in the calculation are $m^*/m = 5.3 \times 10^{-3}$ in the upper curve and $E_g = 6.36$ eV in the lower curve.

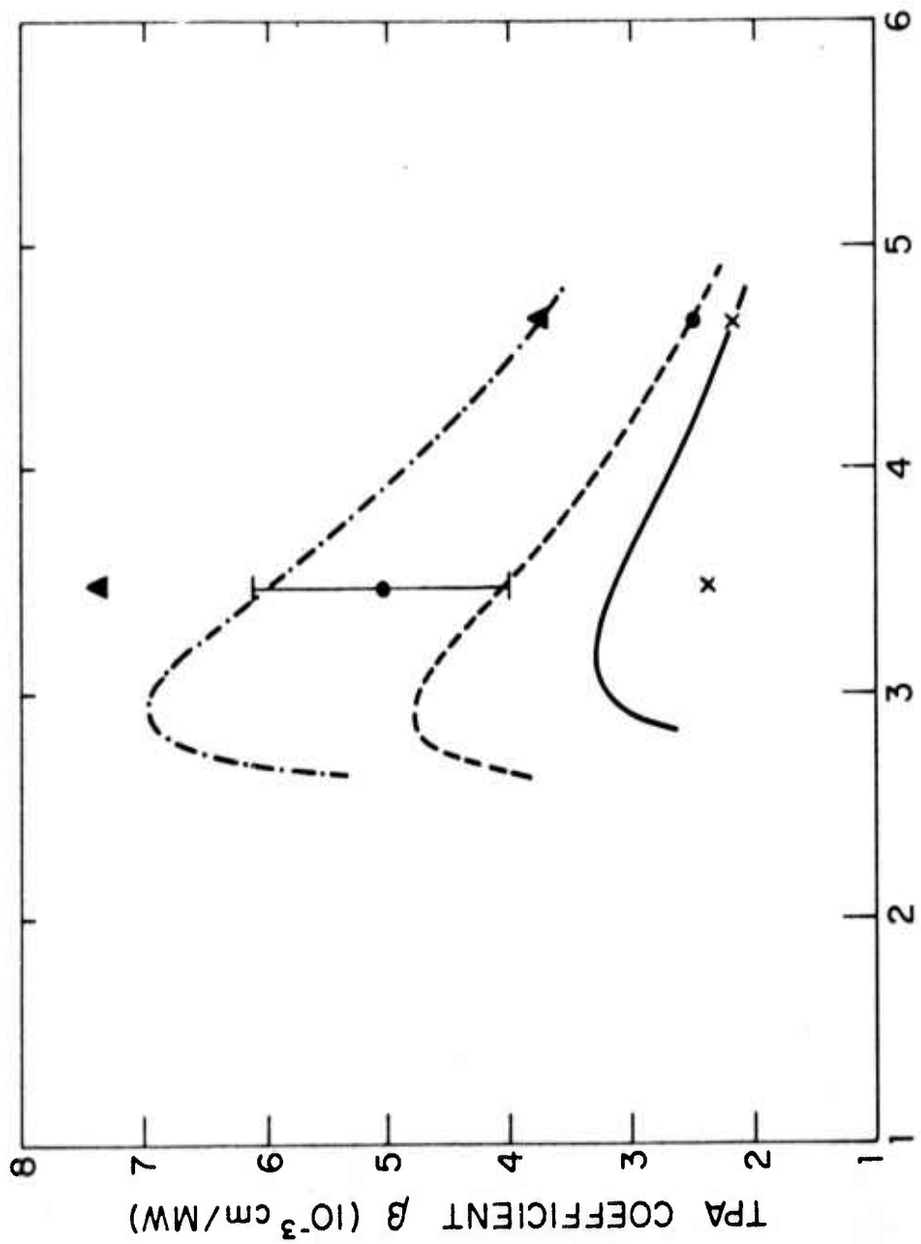

Figure 8. Plot of the input photon energy dependence of β. The experimental results are shown by ▲ for KI, X for RbBr and ● for RbI. The error bar represents only the relative uncertainty. Theoretical dispersion curves are calculated by Eq. (4) using the values of the effective mass found at 266 nm.

multi-photon absorption alone, and melt the sample by plasma heating. Assuming no recombinations during a square picosecond laser pulse, the temperature rise by the free electron absorption is given by

$$\Delta T = \frac{e^2 \tau}{4mc} W E^2 (\Delta t)^2 \frac{1}{1+\omega^2 \tau^2} \quad . \tag{18}$$

Here c is the specific heat, m is the free electron mass, τ is the momentum transfer collision time, Δt is the pulse duration, E is the peak electric field strength, ω is the angular frequency of the light, and W is given by the Keldysh formula [Eq. (3)]. Using Eq. (18) with m^* obtained from the theoretical fit of the TPA measurements at 266 nm and a relaxation time $\tau = 5 \times 10^{-16}$ sec,[12] the electric field threshold for breakdown is calculated. The results for KDP and fused silica are presented along with the available experimental data in Fig. 9.

As discussed in Ref. 12, the breakdown threshold at low frequency is determined by an avalanche multiplication process. In this case a monotonic increase in the breakdown threshold is expected with increasing laser frequency. This is reflected by the experimental data on fused silica, but the contribution to the breakdown from the 3-photon absorption process at the highest frequency is appreciable.

In KDP, the measured breakdown thresholds at 1.06 μm and 532 nm are almost equal. An increase by a factor of two occurs at 355 nm. The Keldysh theory gives breakdown threshold values close to the experimental data at 1.06 μm and 532 nm. In this region the relative contributions of the avalanche ionization and the multi-photon process to the carriers generation have to be considered as discussed by Bräunlich et al.[32]

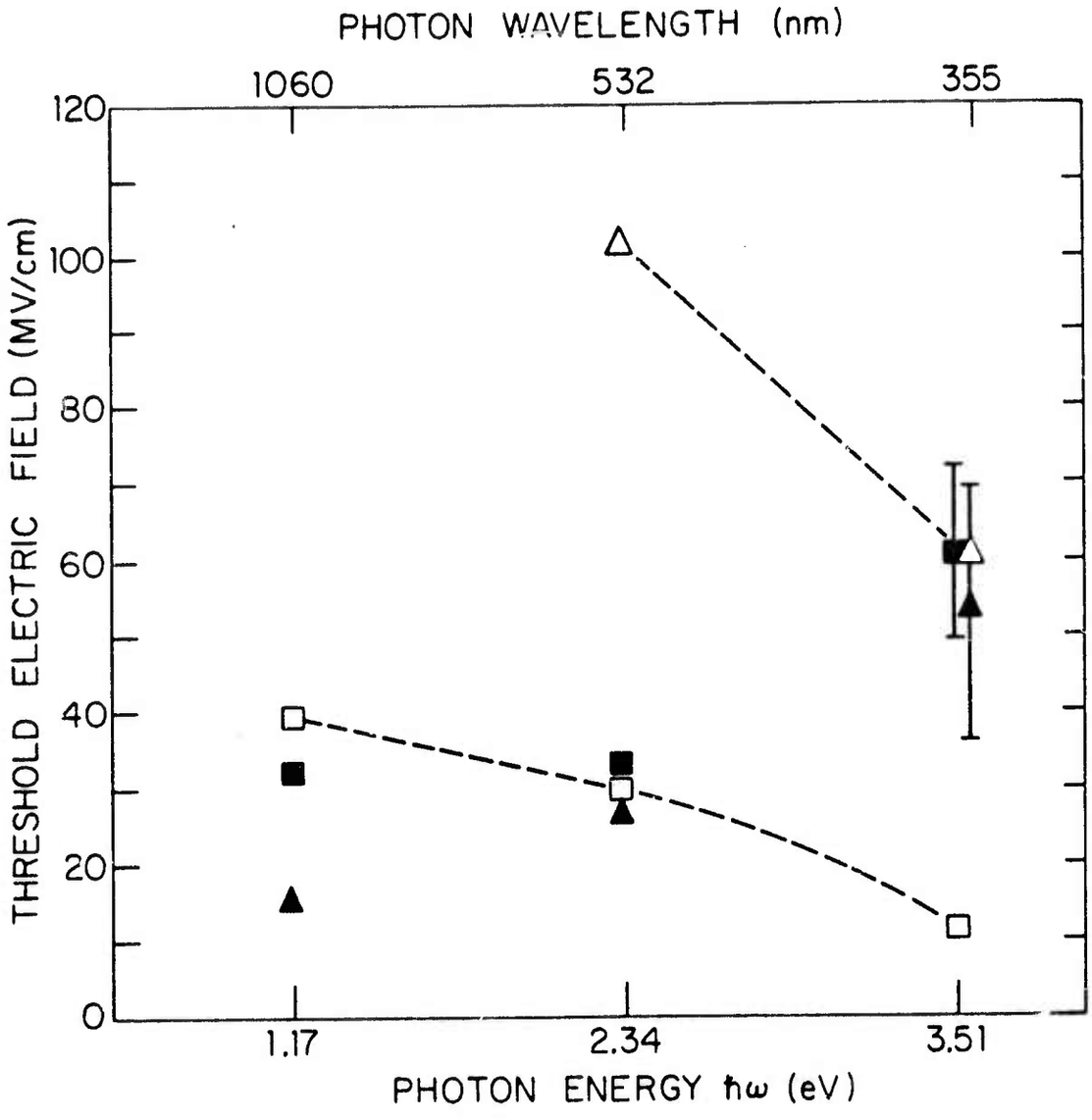

Figure 9. Theoretical calculation according to Eq. (17) (open points) and experimental data (filled points) of the threshold peak electric field for breakdown in KDP (squares) and fused silica (triangles). The dashed curves are used to aid in reading the figure. The breakdown in silica is apparently determined by avalanche ionization, and not by multiphoton absorption.

The larger experimental threshold observed at 355 nm might reflect the nonlinear loss in the sample, which was not taken into account in the determination of the breakdown threshold reported in Ref. 31. For example, with TPA coefficient $\beta = 6 \times 10^{-6}$ cm/MW and tightly focused input beam with intensity $I = 2 \times 10^{12}$ W/cm^2, the percentage loss per 100 μm is as high as 12%. Therefore, nonlinear losses which are not negligible at the high laser intensity used should be carefully considered. In fused silica, the expected nonlinear loss at 355 nm (3-photon absorption) is quite small. Therefore the threshold measured is reliable.

When the damage threshold is determined mainly by the avalanche mechanism, multi-photon absorption before the focal region, where breakdown would occur is an advantage. It lowers the intensity at hot spots, therefore, the possibility of self-focusing and damage is reduced.

In conclusion, we have measured the absolute TPA coefficients of several commonly used u. v. materials and harmonic generating crystals at two frequencies. The frequency dependence is adequately described by the theory of Keldysh. TPA has no appreciable effect on the conversion efficiency in KDP and its isomorphs. We concur in this conclusion reached by Reintjes et al.[14]

Acknowledgement

We express our indebtedness to Mr. S. Maurici for his preparation of samples, and to Dr. L. F. Mollenauer for a U-center doped sample. We also thank Dr. Cid B. de Araujo for sharing equipment and useful discussions, and Mr. Richard Yen for assistance with the measurement.

References

1. M. Goppert-Mayer, Ann. Phys., (Leipz.) 9, 273 (1931).
2. W. Kaiser, and C. G. B. Garrett, Phys. Rev. Lett., 7, 229 (1961).
3. J. M. Worlock, in Laser Handbook, edited by T. Arecchi and F. Schulz-Dubois (North Holland, Amsterdam, 1972).
4. H. Mahr, in Quantum Electronics, edited by H. Rabin and C. L. Tang, V. I (Academic Pres, NY, 1975).
5. V. I. Bredikhin, M. D. Galanin, and V. N. Gorkin, Ups. Fiz. Nauk., 110, 3 (1973) [Sov. Phys.-Ups., 16, 229 (1973)].
6. H. Lotem, W. L. Smith, and J. H. Bechtel, App. Phys. Lett., 28, 389 (1976).
7. H. Lotem and Cid B. de Araujo, Phys. Rev. B, 16, 1711 (1977).
8. H. Lotem and R. T. Lynch, Jr., Phys. Rev. Lett., 37, 334 (1976).
9. N. G. Basov, A. Z. Grasyuk, I. G. Zubarev, V. A. Katulin, and O. N. Krokhin, Zh. Eksp. Teor. Fiz., 50, 551 (1966) [Sov. Phys. -JETP, 23, 366 (1966)].
10. G. C. Bjorklund, L. F. Mollenauer, and W. J. Tomlinson, App. Phys. Lett., 29, 116 (1976).
11. N. Bloembergen, IEEE J. Quantum Electronics, QE-10, 375 (1974).
12. W. L. Smith, J. H. Bechtel, and N. Bloembergen, Phys. Rev. B, 12, 706 (1975).
13. K. Kato, Opt. Comm., 13, 361 (1975).
14. J. Reintjes and R. C. Eckardt, App. Phys. Lett., 30, 91 (1977).
15. L. V. Keldysh, Zh. Eksp. Teor. Fiz., 47, 1945 (1964) [Sov. Phys. -JETP 20, 1307 (1965)].

16. S. S. Mitra, L. M. Narducci, R. A. Shatas, Y. F. Tsay, and A. Vaidyanathan, App. Opt., 14, 3038 (1975).

17. J. H. Bechtel and W. L. Smith, Phys. Rev. B, 13, 3515 (1976).

18. C. Flytzanis, in Quantum Electronics, edited by H. Rabin and C. L. Tang, V. I (Academic Press, NY, 1975).

19. P. D. Maker and T. W. Terhune, Phys. Rev., 137, A801 (1965).

20. W. L. Smith and J. H. Bechtel, J. App. Phys., 47, 1065 (1976).

21. A. L. Smirl, Private Communication.

22. M. Geller, D. E. Altman, and T. A. Detemple, App. Phys. Lett., 11, 221 (1967).

23. J. N. Bradford, R. T. Williams, and W. L. Faust, Phys. Rev. Lett., 35, 300 (1976).

24. W. B. Fowler, Physics of Color Centers edited by W. B. Fowler (Academic Press, NY, 1968).

25. Y. Toyozawa, Exciton lattice interaction--fluctuation, relaxation, and defects formation, in Proc. of the IV Intl. Conf. on Vac. u. v. Radiation Physics, edited by E. E. Koch et al. (Pergamon, Vieweg, Hamburg, 1974).

26. S. A. Akhmanov, R. V. Khokhlov, and A. P. Sukhorukov, Self-focusing, self-defocusing and self-modulation of laser beams, in Laser Handbook, edited by T. Arecchi and F. Schulz-Dubois (North Holland, Amsterdam, 1972).

27. L. F. Mollenauer, G. C. Bjorklund, and W. J. Tomlinson, Phys. Rev. Lett., 35, 1662 (1975).

28. D. Fröhlich, Phys. Rev. Lett., 19, 496 (1967).

29. K. Park, Phys. Rev. Lett., 22, 1426 (1968).

30. J. Reintjes and R. C. Eckardt, IEEE J. Quantum Electronic, QE-13, 791 (1977).

31. W. L. Smith, J. H. Bechtel, and N. Bloembergen, Phys. Rev. B, 15, 4039 (1977).

32. P. Bräunlich, A. Schmid, and P. Kelly, App. Phys. Lett., 26, 150 (1975).

33. Alkali-halides are from the Harshaw Chemical Co., Solon, Ohio 44139. KDP, ADP used at 266 nm are from the Cleveland Crystal Inc., Cleveland, Ohio 44110. KDP and its isomorphs used at 355 nm are from the Quantum Technology Inc., Grand Island, NY 14072. Fused silica is from the Amersil Inc., Hillside, NJ 07205.

34. Linear data including the index of refraction and absorption coefficient of the materials used in this experiment are taken from: Am. Inst. of Physics Handbook, 3rd edition, (McGraw-Hill, NY, 1972). Landolt-Bornstein, Zahlenwert und Funktionen aus Physik· Chemie-Astro-Geophys-Tech. (8) (Springer-Verlag, Berlin, 1962). D. N. Nikogosyan, Kvant. Elektron, 4, 5 (1977) [Sov. J. Quantum Electronics, 7, 1 (1977)]. W. L. Smith, App. Opt., 16, 1789 (1977).

APPENDIX

The relations between the TPA coefficient in different polarization conditions, and the corresponding components of $\chi^{(3)}(-\omega, \omega, \omega, -\omega)$ are obtained by defining the third-order nonlinear polarization. In cubic materials only 4 components of $\chi^{(3)}$ are independent. By using the general permutation rules for $\chi^{(3)}$ and the additional symmetry because we are dealing with only a single laser frequency, we get for the following three cases:

A. the electric field parallel to the crystal x axis with amplitude E_0,

$$\vec{P}^{N.L.}(\omega) = \begin{pmatrix} 3 \chi^{(3)}_{xxxx} E_x^2 E_x^* \\ 0 \\ 0 \end{pmatrix} , \qquad (A1)$$

B. the electric field in the $[1, 1, 0]$ direction with same amplitude E_0,

$$\vec{P}^{N.L.}(\omega) = \begin{pmatrix} 3 \chi^{(3)}_{xxxx} E_x^2 E_x^* + 6 \chi^{(3)}_{xxyy} E_y E_x E_y^* + 3 \chi^{(3)}_{xyyx} E_y^2 E_x^* \\ 3 \chi^{(3)}_{xxxx} E_y^2 E_y^* + 6 \chi^{(3)}_{xxyy} E_x E_y E_x^* + 3 \chi^{(3)}_{xyyx} E_x^2 E_y^* \\ 0 \end{pmatrix} \qquad (A2)$$

C. the electric field is circularly polarized, $\vec{E} = E_0(\hat{x} + i\hat{y})$,

$$\vec{P}^{N.L.}(\omega) = \begin{pmatrix} 3\,\chi^{(3)}_{xxxx} E_x^2 E_x^* + 6\,\chi^{(3)}_{xxyy} E_y E_x E_y^* - 3\,\chi^{(3)}_{xyyx} E_y^2 E_x^* \\ 3i\chi^{(3)}_{xxxx} E_y^2 E_y^* + 6i\chi^{(3)}_{xxyy} E_x E_y E_x^* - 3i\chi^{(3)}_{xyyx} E_x^2 E_y^* \\ 0 \end{pmatrix} \tag{A3}$$

The TPA work done on the material is given by $w = \mathrm{Re}\left\{\frac{\vec{P}\cdot\dot{\vec{E}}^*}{2}\right\}$. The TPA coefficient is defined by

$$\beta = w^2/I^2 . \tag{A4}$$

Using the expression for the laser intensity for linearly polarized light

$$I = \frac{n_0 c}{8\pi} E_0^2 , \tag{A5}$$

and for circularly polarized light

$$I = \frac{n_0 c}{4\pi} E_0^2 , \tag{A6}$$

with the nonlinear polarizations given above, Eqs. (6-8) given in the text are easily obtained.

C. SUMMARY OF WORK ON SUPERCONDUCTING MATERIALS.

Professor M. Tinkham, Principal Investigator.

Three entirely different classes of novel superconducting materials have been studied, and publications have appeared.[1-3]

The first of these are the superconducting layered compounds, such as TaS_2 and $NdSe_2$, both with and without organic intercalates such as pyridine. These compounds have highly anisotropic superconducting properties, the critical field parallel to the plane of the layers being orders of magnitude higher than the perpendicular critical field. There appeared to be some potential for utilizing the high parallel critical field with possibly strong pinning of flux lines between the layers to make superconductors with unique high-field properties. One of the critical questions to be resolved was that of dimensionality: does the material act like a collection of independent 2-dimensional superconducting planes, or is the interplane coupling strong enough to yield 3-dimensional, albeit highly anisotropic, behavior. Prober's experiments were aimed at answering such questions by measuring the critical field as a function of angle with the plane and as a function of temperature, and also of measuring the diamagnetism above T_c associated with thermodynamic fluctuations. The latter appeared to offer particularly direct information about dimensionality, since the temperature dependence in the 2-D and 3-D cases are different. In fact, although the measurements were more extensive and careful than any previous ones, sample-related problems set limits to the definiteness of the conclusions. In particular, warping and crinkling of the planes made the notion of precise parallelism

unrealistic. Nonetheless, from the data we could conclude that the materials do act 3-dimensional over a considerable temperature range on either side of T_c; in fact, no convincing evidence for 2-dimensional behavior was found. Also, the very weak dependence of interplane coupling on the thickness of the organic intercalating layer shows that the coupling is not of a simple tunneling type, which would have an exponential variation. A paper on this work by D. E. Prober (now at Yale) and M. R. Beasley (now at Stanford) has been published.[1]

The work of Powell, Skocpol and Tinkham,[2] was designed to pursue the feasibility of making superconducting materials of superior pinning strength by tailoring the scale of the microstructure to the intervortex spacing, typically hundreds of angstroms. The materials studied were NbN and NbC and intermediate compositions. Fine particles of a Nb-containing compound were prepared by spray drying a suitable solution. These particles were then reduced to the desired compound by heating them in an atmosphere of H_2 mixed with CH_4 or NH_3. They were subsequently pressed and sintered into solid rods, whose superconducting properties (T_c, H_{c2}, J_c) were measured. A wide range of conditions was explored, varying the spray drying technique, solution concentration, etc., varying the temperature and gas mixture for the heat treatment, and then varying the final sintering conditions. With a certain amount of optimization of these many variables, it proved possible to make NbN with pinning properties (as measured by J_c) somewhat superior to the best reported on samples made by more conventional techniques. However, it was hard to retain optimum grain size while obtaining sufficient sintering of particles to make a cohrent solid. Thus, although this work basically supports our initial theoretical notions, this technique

does not appear to offer much promise for the fabrication of practical superconductive materials. The fine particle preparation technique may have wider applicability, however.

The final class of materials worked on is that of superconductive micro-composite wire, produced metallurgically in the way first reported by Tsuei. This wire is typically made by melting together Nb, Sn, and Cu, quenching at such a rate that small Nb grains precipitate from the Cu-Sn solution. Upon drawing, the Nb grains become extremely long, thin filaments (of finite length) embedded in a Cu-Sn solid solution matrix. A suitable heat treatment allows the Sn to react with the Nb filaments, forming a sheath of the high performance superconductor Nb_3Sn. This yields a wire containing thousands of filaments of micron diameter in the cross section of the wire. Because of the fineness of the filaments, the composite is ductile, despite the hardness of the Nb_3Sn. Also, being made by purely macroscopic metallurgical methods, it should be relatively inexpensive, and of interest for applications, such as fusion confinement magnets, requiring large amounts of superconductive wire. An obvious question, however, was whether such a wire containing finite length superconductive filaments in a copper matrix was truly superconductive. On the other hand, a simple theoretical model showed that even if the copper were fully normal, the resistance would be reduced by a factor of order 10^7 below that of the copper matrix, just because of the presence of the very long filamentary superconductive segments. The expected residual resistance would be below the level detectable by conventional instrumentation, and in fact low enough that it would not interfere with practical application.[3] Davidson developed a superconductive voltmeter sensitive enough to detect the expected residual resistance. What he then

found was that at low currents, the material is a true superconductor, the proximity-effect superconductivity in the copper being sufficient to carry the current from one filament to the next. At higher currents (and/or magnetic fields) he found a very small, but finite resistance, similar to that expected theoretically. Moreover, he pointed out the need to invoke notions from percolation theory to obtain an appropriate understanding of the observations. That is, above a percolation threshold estimated to be 15% concentration of superconductor by volume, one expects a continuous superconducting path by mere random close contacts between filaments. This work is at present continued with support from other sources.

The following papers and reports were supported in part by this contract:

1. D. E. Prober and M. R. Beasley, "Fluctuation-induced diamagnetism and dimensionality in superconducting layered compounds: TaS_2 (pyridine) and $NbSe_2$," Phys. Rev. B15, 5245, 1977.

2. R. M. Powell, W. J. Skocpol, and M. Tinkham, "Preparation and superconducting properties of ultrafine powders and sintered compacts of NbC and NbN," Journ. Appl. Phys., 48, 788, 1977.

3. A. Davidson and M. Tinkham, "Phenomenological equations for the electrical conductivity of microscopically inhomogeneous materials," Phys. Rev., B13, 3261-3267, 1976.

4. R. M. Powell, "Preparation and Superconducting of Sintered Compacts of NbN Microcrystallites," Report No. 11, Division of Engineering and Applied Physics, Harvard University, October 1975.

5. A. Davidson, "Applied Superconductivity Amplifiers and Microcomposite Wire," Report No. 12, Division of Engineering and Applied Physics, Harvard University, January 1976.

D. SUMMARY OF WORK ON FRACTURE MECHANICS.

Professor J. W. Hutchinson, Principal Investigator.

Work was completed in two areas during the funding period: (i) large scale yielding crack problems and (ii) near tip elastic-plastic fields for growing cracks.

Extensive numerical results were generated for fully plastic plane stress crack problems for two of the most important crack configurations, the center cracked strip and the edge cracked strip in bending. These solutions can be used in an approximate way to construct simple formulas governing fracture conditions for the full elastic-plastic configuration.[1] The formulas reduce at low load to the elastic results and at high load they merge into the fully plastic solution. To assess the accuracy of the simple formulas some full scale finite element calculations were carried out. The agreement with the simple formula predictions was excellent. This work is reported in the paper by C. F. Shih and J. W. Hutchinson.[2]

For the first time, stress and strain fields have been found at the tip of a crack growing steadily in an elastic-plastic strain hardening material. The material is characterized by a J_2 flow theory of plasticity together with a bilinear effective stress-strain curve. All three cases of interest were considered, i.e., anti-plane shear, plane stress and plane strain. Perhaps the most important finding is that a small amount of strain hardening leads to a relatively strong singularity compared to the ideally plastic case. It is still true that the strain fields at the crack tip are not nearly as singular in the growing case as in the stationary case. But the theoretical results suggest that it still may be possible to employ the concept of a growing crack-tip stress intensity

factor to analyze stably growing cracks in analog to the stress intensity concept that has been so successful in treating stationary cracks. This work is summarized in the paper by J. C. Amazigo and J. W. Hutchinson.[3]

The following papers and reports were supported in part by this contract:

1. J. W. Hutchinson, "Bounds and self-consistent estimates for creep of polycrystalline materials," Proc. R. Soc. Lond. A348, 101-127, 1976.

2. C. F. Shih and J. W. Hutchinson, "Fully plastic solutions and large scale yielding estimates for plane stress crack problems," J. Eng. Mat. and Tech., 98, 289-295, 1976.

3. J. C. Amazigo and J. W. Hutchinson, "Crack tip fields in steady crack growth with linear strain hardening," Report S-18, Division of Engineering and Applied Physics, Harvard University, June 1976, to be published in J. Mech. Physics Solids.